Proceedings of the ASME 2019 Conference on Smart Materials, Adaptive Structures and Intelligent Systems
SMASIS2019
September 9 - 11, 2019, Louisville, Kentucky , USA

SMASIS2019-5625

CHORD MORPHING FOR HELICOPTER ROTOR BLADES

Johannes Riemenschneider, Christoph Balzarek
German Aerospace Center (DLR)
Institute of Composite Structures and Adaptive Systems
Lilienthalplatz 7
38108 Braunschweig
Germany

Berend G. van der Wall, Rohin Kumar Majeti
German Aerospace Center (DLR)
Institute of Flight Systems
Lilienthalplatz 7
38108 Braunschweig
Germany

ABSTRACT

Since helicopter rotors have different demands from different flight stats, the final design is always a compromise between flight stats such as hover and fast forward flight. Two of the design parameters are twist and chord length. This paper is giving some reasoning from rotor simulations on what twist and chord length should look like in order to increase performance in hover or forward flight. The result is, that the inboard chord length should be much larger for hover than for forward flight. This paper is presenting a structural concept, that can enable a helicopter rotor blade to change its chord length.

Keywords: morphing, rotor, helicopter, trailing edge, chord extension

1 Introduction

Presently, the design of helicopter rotor systems is highly constrained by the demanding and widely varying operating conditions they must endure. These constraints require significant compromise in the design of the blade geometry between competing flight conditions, for example, between hover and forward flight, resulting in blades that are less than optimally efficient in both flight conditions. Morphing rotor blades could address this issue, by changing the rotor blade shape according to the demands of the flight states. From rotor dynamic calculations it is known, that longer chord length at the blade root and increased pre-twist [1] would increase the performance in hover, whereas shorter chord and less twist is beneficial for fast forward flight. Some concepts have been shown in literature, that mainly focus on a uniform extension of the blade chord at a particular region of a blade [2, 3, 4]. Within this paper a performance calculation for blades with different blade shapes is given to motivate the design of a morphing rotor blade that can change the chord length in the root region. The motivational section is followed by a presentation of a structural concept for such a chord morphing. This concept shows a trailing edge that can be extended, where the amount of the extension is varying over span. There is a pivot point at around 60% R and the chord extension is linearly increasing all the way to the blade root at 22% R. In this region an auxiliary spar is dividing the blade in a conventional rigid front part and a morphing rear part. The structural design of this rear part is the main focus of this paper. It consists of two components: a flexible skin as well as an inner support structure. The idea is to use rubber like EPDM material for the skin reinforcing the skin in span wise direction by fibers. The skin thickness will be designed by shape accuracy on one end and actuator force to extend the mechanism and stretch the skin at the same time. The underlying support structure consists of vertical GFRP extending in span wise direction. Design parameters for those webs are the distance, which relates to the skin design, as well as the thickness of the members, which influences the overall stiffness of the design. The publication will present a workflow, in which the rotor is being structurally designed coming all the way from a generic CAD model, considering cg location as well as

elastic deformation of the elastic skin and calculating the cross section wise stiffness of structure. This section wise approach is followed by the setup of a beam model of the blade for dynamic analysis as well as the setup of a 3D model for strength analysis as well as aeroelastic coupling.

Figure 1 is showing the basic principal of the morphing concept, which is being followed in this paper.

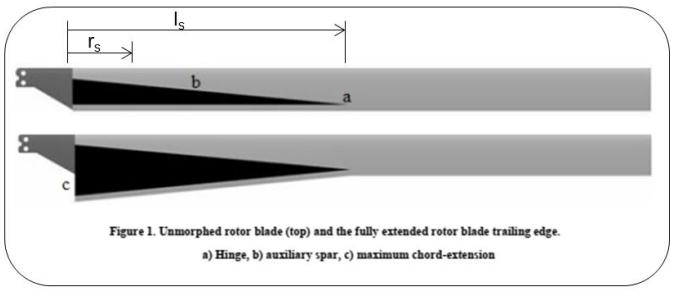

Figure 1. chord morphing overall concept

2 Potential of chord extension

2.1 table of symbols

symbol	description
c_d	Drag coefficient
c_l	Lift coefficient
c_l/c_d	Lift to drag ratio
c_P	rotor power coefficient
c_T	thrust coefficient
c_T/σ_{BL}	blade loading coefficient
FM	figure of merit
M	Mach number
r	radial position
T	thrust
α	angle of attack
$\Delta\theta_{tw}$	additional blade twist
η	chord extension deflection
σ_{BL}	blade section solidity
θ_{tw}	pretwist

The "optimum hovering rotor", described in classical literature [5] as having the best possible figure of merit (FM), has a hyperbolic twist and hyperbolic chord distribution along the rotor blade span. The hyperbolic twist distribution induces uniform inflow over the rotor disk and thus, minimizes the induced power. The hyperbolic chord distribution maximizes the sectional lift-to-drag ratio throughout the span and thus, minimizes the profile power. Since hyperbolic distributions are difficult to achieve, it is more common to find linear twist and linearly tapering chord length in rotor blades as an approximation.

The goal of the analytical studies is to investigate the potential performance gains of the previously described chord morphing in relation to that of a baseline rotor. Chord morphing with and without deflection of the chord extension and its combination with twist morphing were evaluated with respect to maximizing the hover figure of merit (defined later). It is to be noted that chord deflection modifies the chord line orientation and hence the aerodynamic blade twist. The analysis was performed using the blade-element momentum theory (BEMT). To the basic BEMT, realistic refinements such as compressibility and static stall of airfoil polars were implemented. Blade tip loss was considered to be effective from 0.9R and has been assumed to be constant with thrust. The Bo105 main rotor, assumed to be rigid, was taken as the baseline rotor. The baseline blade section solidity is $\sigma_{BL} = 0.07$. The reference thrust of $T = 22,073N$, or a thrust coefficient of $C_T = 0.005$ was used giving a blade loading coefficient of $C_T/\sigma_{BL} = 0.0714$. Since no blade motion was considered, aerodynamic moments about the quarter chord were not required. Figures 2 - 4 shows the good correlation between the airfoil coefficients' analytical model and the wind tunnel data for the baseline rotor for the Mach numbers of interest in hover.

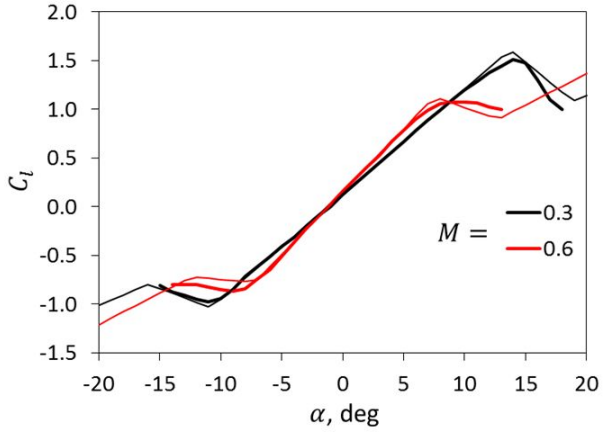

Figure 2. Lift coefficients of wind tunnel data (thick lines) and analytical model (thin lines)

The BEMT computations were performed using 18 blade elements distributed along the span with smaller element widths near the root cutout and blade tip to capture root and tip losses accurately (Figure 5). Collocation points within each element give the locations where local velocities, lift, and drag coefficients are evaluated. The figure of merit (FM) which is the main performance parameter is defined as

$$FM = \frac{c_{P,ideal}}{c_P}; c_{P,ideal} = \sqrt{\frac{c_T^3}{2}}$$

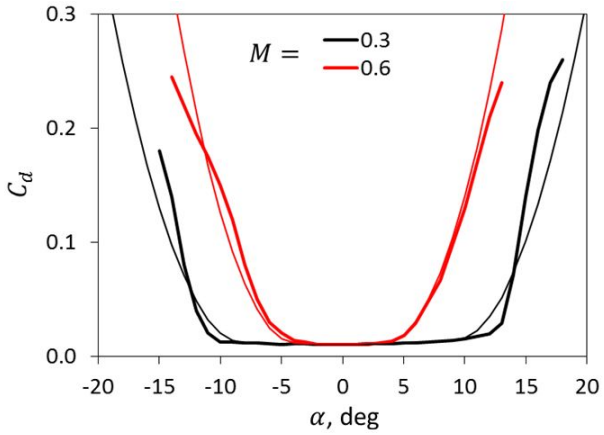

Figure 3. Drag coefficients of wind tunnel data (thick lines) and analytical model (thin lines)

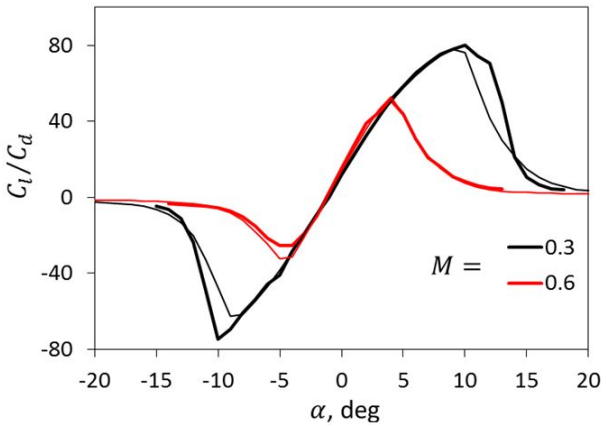

Figure 4. Lift-to-drag ratio of wind tunnel data (thick lines) and analytical model (thin lines)

where c_P is the actual rotor power computed. The results presented here are a summary of those already given in [6]:

The baseline rotor has a pretwist of $\theta_{tw} = -8deg/R$. Giving it additional linear twists, the FM is computed for a range of blade loadings. The computed FM is shown in Figure 6. For the baseline rotor, the FM at nominal thrust is $FM = 0.680$. With an additional twist of $\Delta\theta_{tw} = -8deg/R$, $FM = 0.691$ can be achieved. The highest achievable $FM = 0.808$ is obtained at an additional twist $\Delta\theta_{tw} = -16deg/R$ at a blade loading $C_T/\sigma_{BL} = 0.140$.

The FM for combined chord and twist morphing is shown in Figure 7. 100% chord extension at the root and a hinge position of 0.6R is used along with varying twist. The airfoil polars for the new sections are assumed to remain the same as the baseline. The highest achievable figure of merit has increased for this case compared to the baseline rotor. $FM = 0.818$ is obtained

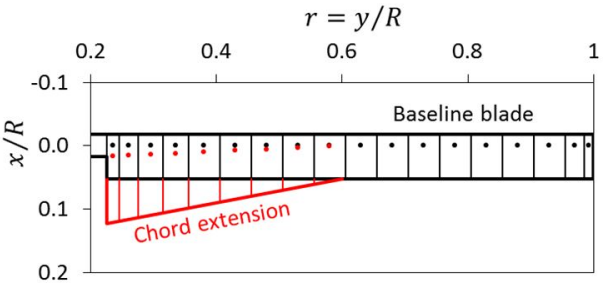

Figure 5. Baseline blade discretization and chord morphing

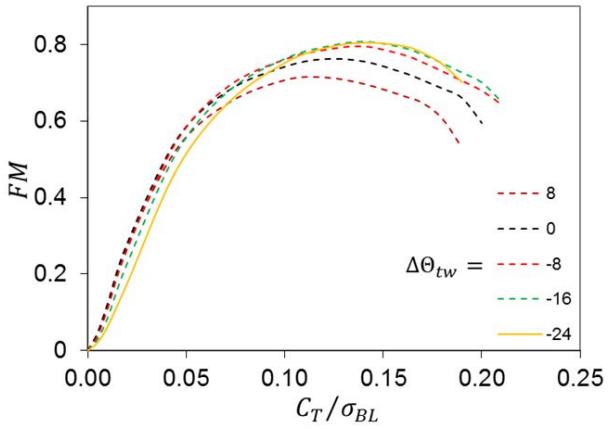

Figure 6. FM of baseline rotor with twist morphing

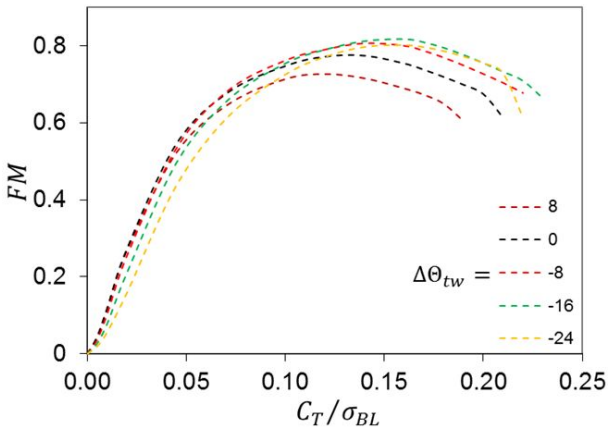

Figure 7. FM with 100% chord and twist morphing

at an additional twist of $\Delta\theta_{tw} = -16deg/R$ at a blade loading $C_T/\sigma_{BL} = 0.160$. In addition, a larger maximum thrust is reached because of the larger blade surface in the chord morphing case.

Deflecting the deployed part of the chord, an additional twist is introduced in the inboard region, better approximating

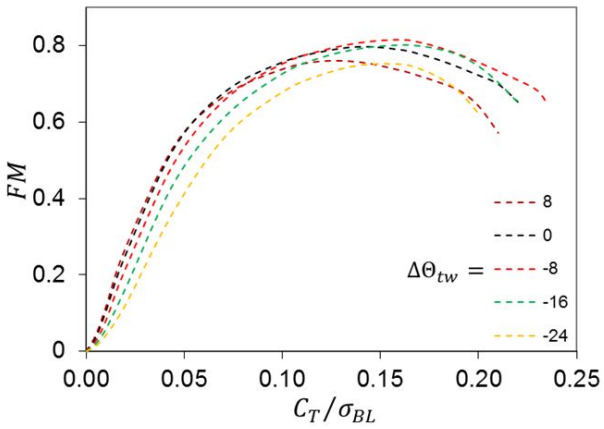

Figure 8. FM with 100% chord, 15 deg deflected, and twist morphing

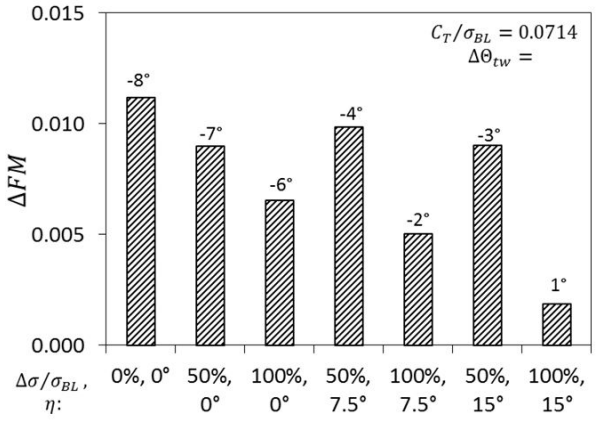

Figure 9. Gains in FM relative to the baseline blade, nominal thrust, 0.6R hinge position

the hyperbolic twist. Results for the 100% chord extension deflected by $\eta = 15deg$ is shown in Figure 8. The highest possible FM = 0.816 is achieved at an additional twist of only $\Delta\theta_{tw} = -8deg/R$ at a blade loading $C_T/\sigma_{BL} = 0.160$.

Figure 9 shows the gains in FM from various combinations of chord extension and chord deflection at the nominal thrust. The biggest gains can be obtained by twisting alone but it requires $\Delta\theta_{tw} = -8deg/R$ additional twist. The second largest gains are obtained with a 50% chord extension deflected by $\eta = 7.5deg$, which requires only $\Delta\theta_{tw} = -4deg/R$ additional twist; and the undeflected chord extension of 50%, but again $\Delta\theta_{tw} = -7deg/R$ additional twist is needed there.

At a higher thrust level of $C_T/\sigma_{BL} = 0.160$ (Figure 10), it can be seen that the achievable gains are much larger than those at the design thrust. The 100% chord extension, with and without deflection, gives the largest increment in gains. This is because the morphing with a larger blade area allows for larger thrust

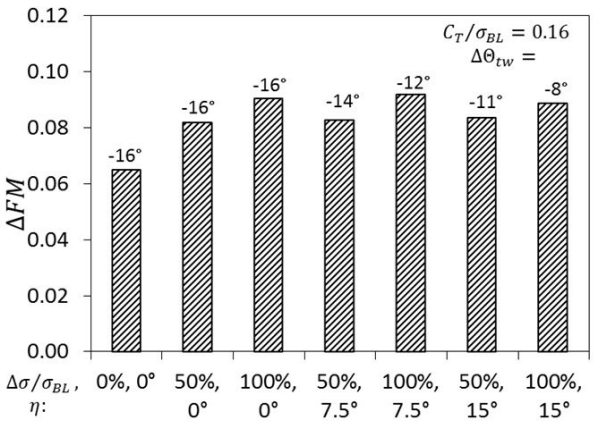

Figure 10. Gains in FM relative to the baseline blade, high thrust, 0.6R hinge position

with less control angle, thus more margin relative to stall and the smaller angles of attack also reduce the profile drag. All optimum points require more additional twist morphing of the blade than at design thrust, which is caused by the high loading.

3 Structural Design of flexible trailing edge

A rear spar is located in the trailing edge and can be swept back around a pivot point, which is located at 60% blade radius. At the innermost radial location of the aerodynamic profile (at 22% blade radius) this spar is actuated perpendicular to the radial direction by an actuator. In this region the blade consists of a conventional front structure, made of a conventional C-spar, a counterweight and a conventional load bearing composite skin. This conventional region ends at a diagonally implemented auxiliary spar, which is the starting point for the morphing rear part of the blade. In this rear part, an elastic skin is used, which allows the morphing to take place. Unidirectional reinforcements in the radial direction account for the centrifugal loads on the skin. In order to maintain the blade shape of the soft skin, a number of support elements are used. They keep the distance between the upper and lower skin and transfer aerodynamic loads from the skin into the auxiliary spar and a support at the root. The trailing edge rear spar is carried out as a stiff component which transfers the actuator force applied at the blade root and transmits the deflection all the way up to the pivot point. The described concept is shown in Figure 11.

For the blade design an optimization routine has been established, which is able to design profile cross sections. For the design of the concept, cross sections at 8 radial positions were defined between 22% and 60% radius, the results of which were interpolated over the entire morphing range. The optimization routine starts with a model generator in which all design variables are stored parametrically. The FE tool imports the surfaces

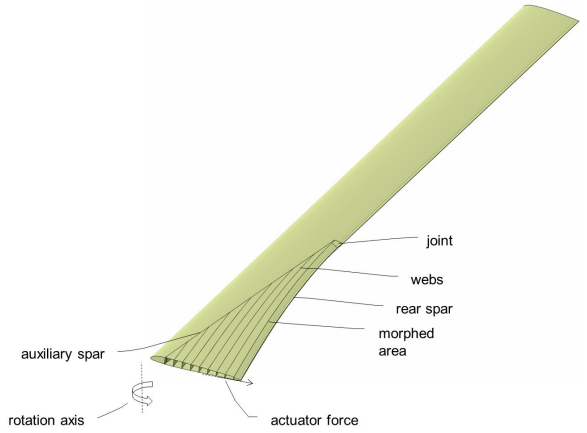

Figure 11. chord morphing concept

and volumes of the CAD model and discretizes them for the calculation. Subsequently, the layer structure is defined for the individual components of the concept. In a first loop, the center of gravity of the model is determined and the counterweight is adjusted until the center of gravity reaches the c / 4-line. In a second loop, the calculation of the Inertia Moments, Mass Properties, as well as the calculation of the stiffnesses takes place. The result of this loop are the rotor blade properties, such as the positions of the individual axes (center of gravity, shearcenter, tension center) and stiffnesses. These values can then be used to calculate the blade dynamics and stability analysis. This process is visualized in Figure 12.

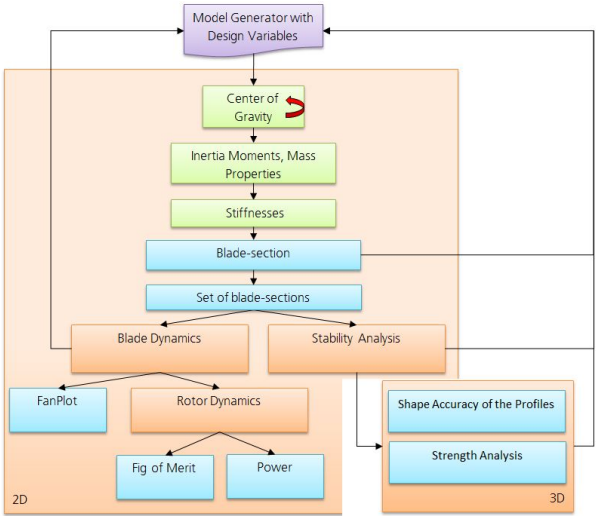

Figure 12. Process of trailing edge dimensioning

To evaluate the shape accuracy of the profiles two different approaches are used. One is a local approach, which is looking at the wrinkling of the skin due to the pressure on the outside at a given substructure. The main task here is to find a suitable compromise between a low in plane stiffness of the elastic material, for a better actuation and a low out of plane deformation due to the aerodynamic loads. The in plane stiffness thus defines the size and thus weight of the required actuator. The out-of-plane deflection of the skin changes the surface of the profile, which has a negative effect on the aerodynamic properties. For the concept presented, the elastic skin is stretched by over 160% with a 100% chord extension. Here, a thin sheet of EPDM material, between 0.5mm and 1.5mm is used, which allows strains up to 700%. Likewise, the use of a pre-stressed skin was considered which, however, has a negative effect on the out of plane displacement with increasing elongation. Therefore, the prestressing is kept as small as possible, which in turn has a positive effect on the required actuator force and the material fatigue of the skin itself. FE analysis of the skin behaviour under pressure as a function of the web distance and the skin thickness was carried out at constant ambient pressure of 13 kPa. Results of this study can be seen in figure 13. Two morphing states were examined for this analysis: fast-forward (chord extension 0%) and hover (chord extension 100%). Figure 14 shows one example result of skin deflection with varying web spacing and different skin thicknesses.

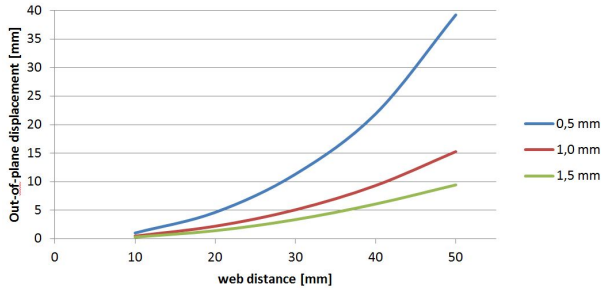

Figure 13. Deflections over web distance for skins with different skin thickness.

On top of this investigation on the local effects of the skin, there was also an approach to look at the overall deflections of the structure in a aeroelastic coupling. The substitution of the rigid skin and the foam core, a conventional rotor blade, by an elastic skin with discrete points of support, results in a significant loss of rigidity of the trailing edge. The aerodynamic loads have to be carried by webs mounted at two points in the auxiliary spar and the guide in the root area. The resulting out-of-plane displacement lead to a non-negligible change in the shape of the airfoil. This changes the resulting pressure distribution across the profile. In order to be able to map this changed load, the structural

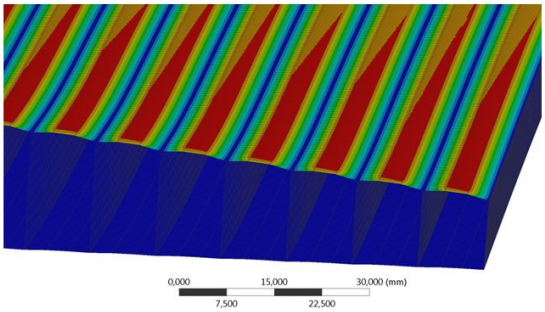

Figure 14. FEA result of the skin deflection due to pressure loading for rib distance of 10 mm.

design process is supplemented by an iterative process, which comprises five steps:

1. Creation of structural model
2. Calculation of actuator-induced deflection in ANSYS
3. Calculation of pressure distribution of the deflected trailing edge in XFOIL
4. Calculation of the resulting deflection with aerodynamic pressures in ANSYS
5. Evaluation of deflected airfoil geometry

This was carried out for several different flight conditions: hover as well as fast forward flight. For fast forward flight, three azimuth positions were chosen for aerodynamic loading. The hover is assumed to be identical in every position. In a CAD program, the blade structure was created as a shell model. The model itself is in turn parameterized so that changes can be automated within the scope of a sensitivity study or optimization. In contrast to the previously presented optimization routine (Figure 12), this is the entire 3D model of the concept. In Ansys then followed the discretization of the model. Furthermore, the material properties and the layer structure of the individual components were defined here. Two models were provided by CAD for the simulation. First, an unmorphed model for the fast forward flight, which corresponds to the normal rotor blade profile, but has a modified, internal structure. The second model corresponds to the fully morphed rotor blade with a chord deflection of 100% at 22% radial position, for hovering. Also with changed, internal structure. These two models are unloaded and represent the reference profiles for the pressure calculation. On the aerodynamic side, XFOIL was used. Since it is a 2D based program, 8 different profile cross sections in the tension direction between 22% and 60% radius were determined to calculate the pressure distributions of both models. From the individual pressure distributions, a global pressure field was interpolated, which represents the starting conditions for the FE simulation. For the coupling, new cross sections are extracted from the deformed blade and a new pressure calculation in X-Foil is carried out. This process

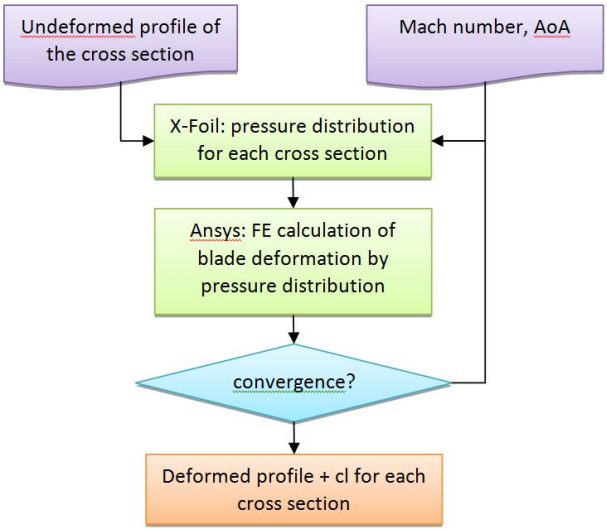

Figure 15. Flowchart of the aero-structural coupled simulation.

can be repeated until the displacement of the trailing edge converges. Normally three to four iterations were required until the changes were kept at 1%. One representative result can be found in figure 16.

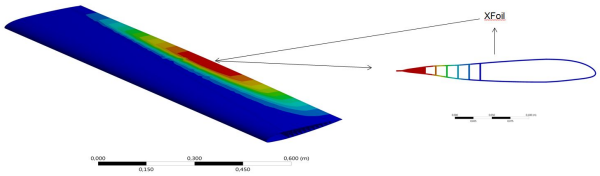

Figure 16. Result of an aeroelastic coupling.

4 Conclusions

This paper shows the high potential of chord morphing for helicopter rotors in order to reduce the power requirement especially in hover. Also a concept for the structural realisation of such a chord morphing was presented on how it can actually be done. The simulation framework for the structural design was shown as well as the results of some structural and aeroelastic analysis.

5 Future Work

Next steps are the consequent optimisation of the design in the numerical framework presented. Thus optimisations will include flight performance calculations as well as strength calculations. In a second step the design and manufacturing of a demon-

strator is planned, which will allow the testing of this concept in a whirltower experiment as well as in a none rotating wind tunnel. Data of these experiments will help to verify the numerical results.

ACKNOWLEDGMENT

This work was funded by the European Research Council (ERC) under the European Union's Horizon 2020 research and innovation programme, as part of the Shape Adaptive Blades for Rotorcraft Efficiency (SABRE) programme (grant agreement No 723491).

REFERENCES

[1] Salvatore Ameduri, Antonio Concilio, and Bernardino Galasso. Modeling and design of an experimental demonstrator of blade twist through the sma technology. SMASIS 2019, September 2019.

[2] S. Barbarino, F. Gandhi, and S.D. Webster. Design of extendable chord sections for morphing helicopter rotor blades. Journal of Intelligent Material Systems and Structures, 22(9):891–905, 2011.

[3] Patrick Moser, Silvestro Barbarino, and Farhan Gandhi. Helicopter rotor-blade chord extension morphing using a centrifugally actuated von mises truss. Journal of Aircraft, 51(5):1422–1431, 2014.

[4] Farhan Gandhi and Eric Hayden. Design, development, and hover testing of a helicopter rotor blade chord extension morphing system. Smart Materials and Structures, 24, 03 2015.

[5] A. Gessow and G.C. Myers. Aerodynamics of the Helicopter. Frederick Ungar Publishing Co., New York, 1967.

[6] J. Rauleder, B. G. van der Wall, A. Abdelmoula, D. Komp, S. Kumar, V. Ondra, B. Titurus, and B. K. Woods. Aerodynamic performance of morphing blades and rotor systems. AHS 74th Annual forum and Technology Display, May 2018.